LAWRENCE
LIVERMORE
NATIONAL
LABORATORY

LLNL-CONF-816457

Discrete Empirical Interpolation Method based Dynamic Load Model Reduction

N. Duan, J. Zhao, X. Chen, B. Wang, S. Wang

November 5, 2020

IEEE PES General Meeting 2021
Washington, DC, United States
July 25, 2021 through July 29, 2021

Disclaimer

Discrete Empirical Interpolation Method based Dynamic Load Model Reduction

Nan Duan, Junbo Zhao†, Xiao Chen, Bin Wang‡, Song Wang††
Lawrence Livermore National Laboratory, Livermore, CA
†*Mississippi State University*, Starkville, MS
‡*National Renewable Energy Laboratory*, Golden, CO
††*PacifiCorp*, Porland, OR
duan4@llnl.gov; junbo@ece.msstate.edu; chen73@llnl.gov; Bin.Wang@nrel.gov; Song.Wang@pacificorp.com

***Abstract*—Dynamic load models add significant complexity to bulk power system time-domain simulations. The complexity is due to the large number of ordinary differential equations (ODEs) introduced by the dynamic load components such as induction motors. It is challenging to derive reduced-order models (ROMs) for dynamic loads due to the nonlinear functions in their governing equations. This paper applies the discrete empirical interpolation method enhanced proper orthogonal decomposition (DEIM-POD) to approximate the full dynamic load model with the ROM that minimizes the projection error of the nonlinear functions in dynamic load ODEs onto their dominant modes. This approach only requires evaluation of nonlinear functions at selected observation points. The observation points selected by DEIM also provide information for screening critical load buses where dynamic load model parameters contribute the most to the accuracy of ROM across multiple contingencies. The proposed approach is validated on IEEE 9-bus, WECC 179-bus and 2384-bus Polish systems.**

***Index Terms*—dynamic load model, reduced-order model, time-domain simulation, nonlinear function, ordinary differential equation, bulk power system**

I. Introduction

Time-domain simulation is the essential tool for assessing power system dynamic security. A large number of differential algebraic equations (DAEs) need to be solved for different contingencies under different operation conditions to help system operators identify contingencies that would cause instability. With increasing penetration of distributed energy resources (DERs) and controllable loads, this task has become more challenging due to the computational burden introduced by dynamic load models [1] and the difficulty of maintain accurate parameters for a large number of loads [2].

Dynamic load models are becoming the new focus of bulk power system dynamic performance studies [3]. Unlike generation units, which have relatively accurate parameters for simulations, dynamic load models are defined in an aggregated manner, and thus subject to large uncertainties. In fact, it has been reported that poor dynamic load models could have system-wide impacts on voltage stability evaluation [4]. As dynamic load models are becoming more complex than ever, it is appealing for utilities to have reduced-order models (ROMs) which would help limit the dimension of parameter space for model tuning and reduce the time for performing time-domain simulations.

There have been applications of ROMs to generation units. For example, generator coherency group based approaches leverage the insights gained from small signal stability to perform model reduction [5]. Projection based approaches focus on identifying a low-dimensional basis that state variables can project onto [6]–[8]. There are also linearization based approaches [9], [10]. However, the nonlinear functions in power system models require the full state space to evaluate. Therefore, efficient model reduction technique for the nonlinear functions in power systems is still an open research topic. Also, although the ROMs of generation units have been extensively studied, the investigation about dynamic load ROM is still scarce. Since in the bulk power system there are often significantly more load buses than generator buses, it is important to develop techniques for dynamic load model reduction.

The recent advancements in ROM have combined the proper orthogonal decomposition (POD) [11] with the a hyper-reduction method, discrete empirical interpolation method (DEIM) [12]. DEIM-POD shares similar idea with the gappy POD [13] method, which sparsely selects observation points from the full state space to evaluate the nonlinear functions. DEIM introduces an optimal selection procedure of the observation points so that the projection error of the nonlinear functions is minimized [14]. DEIM provides a great solution for dynamic load model reduction because it not only effectively reduces the number of nonlinear function evaluations but also identifies the critical load locations where the parameters are important for the accuracy of dynamic load ROMs.

The contribution of this work is twofold. First, DEIM is applied to the nonlinear functions of the dynamic load models of 3 systems with different scales. Second, this work uses the

This work was supported in part by the U.S. Department of Energy (DOE), Office of Electricity, Advanced Grid Modeling program and in part under the auspices of the U.S. Department of Energy by Lawrence Livermore National Laboratory under Contract DEAC52-07NA27344 with IM release number LLNL-CONF-816457-DRAFT. It was authored in part by the National Renewable Energy Laboratory, operated by Alliance for Sustainable Energy, LLC, for the U.S. DOE under Contract No. DE-AC36-08GO28308. The views expressed in the article do not necessarily represent the views of the DOE or the U.S. Government. The U.S. Government retains and the publisher, by accepting the article for publication, acknowledges that the U.S. Government retains a nonexclusive, paid-up, irrevocable, worldwide license to publish or reproduce the published form of this work, or allow others to do so, for U.S. Government purposes.

observation points selected by DEIM to identify the critical locations for maintaining dynamic load parameter accuracy.

The remainder of this paper is organized as follows: Section II describes DEIM algorithm; Section III describes the dynamic load model and its model reduction formulation with DEIM; Section IV describes the setup of the simulation and system characteristics; Section V presents case studies using the proposed model reduction approach; finally Section VI draws conclusions and discusses future work.

II. Discrete Empirical Interpolation Method

A. Proper Orthogonal Decomposition

With a dynamical system expressed in ordinary differential equation (ODE) form,

$$\dot{\mathbf{x}} = \mathbf{A}\mathbf{x} + \mathbf{F}(\mathbf{x}, \mathbf{u}) \tag{1}$$

where $\mathbf{A} \in \mathbb{R}^{n\times n}$ is the linear operator on state variables $\mathbf{x} \in \mathbb{R}^n$; $\mathbf{F} \in \mathbb{R}^n$ is the nonlinear operator on states $\mathbf{x}$ and input variables $\mathbf{u} \in \mathbb{R}^n$.

A ROM can be constructed using projection based techniques. The orthonormal basis $\mathbf{V_k} \in \mathbb{R}^{n\times k}$ of the trajectories of the state variables defined in (1) can be found through applying singular value decomposition (SVD) to the snapshot matrix of state variables $\mathbf{X} = [\mathbf{x_1}, ..., \mathbf{x_{n_t}}]^T \in \mathbb{R}^{n\times n_t}$ that contains n_t time snapshots,

$$\mathbf{X} = \mathbf{V}\mathbf{\Sigma}\mathbf{W}^T \tag{2}$$

where the diagonal elements of $\mathbf{\Sigma} = \text{diag}(\sigma_1, ..., \sigma_r) \in \mathbb{R}_{r\times r}$ can be utilized to determine the dominant modes of the trajectories. With a chosen threshold σ_{thd}, mode i with $\sigma_i < \sigma_{thd}$ can be omitted and $k < r$ modes are kept to construct the trajectories. This construction requires the basis $\mathbf{V_k} = [\mathbf{v_1}, ..., \mathbf{v_k}] \in \mathbb{R}^{n\times k}$.

The state variables can be projected onto the reduced basis, i.e. $\mathbf{x} = \mathbf{V_k}\tilde{\mathbf{x}}$. Therefore, using the orthonormal property $\mathbf{V_k}^T\mathbf{V_k} = \mathbf{I}$, the ROM model with states variables $\tilde{\mathbf{x}} \in \mathbb{R}^k$ can be expressed as,

$$\dot{\tilde{\mathbf{x}}} = \mathbf{V_k}^T\mathbf{A}\mathbf{V_k}\tilde{\mathbf{x}} + \mathbf{V_k}^T\mathbf{F}(\mathbf{V_k}\tilde{\mathbf{x}}, \mathbf{u}) \tag{3}$$

Although the state space dimension in (3) is reduced to $k < n$ and $\mathbf{V_k}^T\mathbf{A}\mathbf{V_k}$ can be pre-computed and reused for each integration step, the inevitable computational complexity comes with the nonlinear function $\mathbf{F}(\mathbf{x}, \mathbf{u})$ because its evaluation requires the original state variables $\mathbf{x}$.

B. Discrete Empirical Interpolation Method

To reduce the complexity of nonlinear function evaluations, DEIM constructs a second basis by applying SVD to the trajectory of $\mathbf{F}(\mathbf{x}, \mathbf{u})$. Similar to the way the reduced basis $\mathbf{V_k}$ of the state space is chosen, a threshold can be defined to only keep the dominant modes of $\mathbf{F}(\mathbf{x}, \mathbf{u})$. Let $\mathbf{U} \in \mathbb{R}^{n\times m}$ be a matrix with orthonormal columns as the vectors in the reduced basis of the trajectories of $\mathbf{F}(\mathbf{x}, \mathbf{u})$, then a matrix $\mathbf{P} = [\mathbf{e}_{p_1}, ..., \mathbf{e}_{p_m}] \in \mathbb{R}^{n\times m}$ can be constructed to minimize the projection error of $\mathbf{F}(\mathbf{x}, \mathbf{u})$ onto $\mathbf{U}$. In $\mathbf{P}$, the i-th column $\mathbf{e}_{p_i}$ is an unit vector with the p_i-th element equals to 1 and all other elements equal to 0. With the constructed $\mathbf{P}$, the n-dimensional nonlinear function can be interpolated as,

$$\mathbf{F}(\mathbf{x}, \mathbf{u}) \approx \mathbf{U}(\mathbf{P}^T\mathbf{U})^{-1}\mathbf{P}^T\mathbf{F}(\mathbf{x}, \mathbf{u}) \tag{4}$$

Since DEIM chooses m observation points from the n nonlinear functions, only m elements of $\mathbf{F}(\mathbf{x}, \mathbf{u})$ need to be evaluated, which reduces computational burden of evaluating the full $\mathbf{F}(\mathbf{x}, \mathbf{u})$. The way to construct $\mathbf{P}$ is detailed in Algorithm 1 [15].

Algorithm 1: DEIM

Input: $\mathbf{U} = [\mathbf{u}_1, ..., \mathbf{u}_m] \in \mathbb{R}^{n\times m}$
Output: $\mathbf{P} = [\mathbf{e}_{p_1}, ..., \mathbf{e}_{p_m}] \in \mathbb{R}^{n\times m}$
$[\rho, p_1] = \max|\mathbf{u}_1|$;
$\mathbf{P} = [\mathbf{e}_{p_1}]$;
for $i = 2$ *to* m **do**
  solve $\mathbf{P}^T\mathbf{U}(1 : i-1, :)\mathbf{c} = \mathbf{P}^T\mathbf{u}_i$ for $\mathbf{c}$;
  $\mathbf{r} = \mathbf{u}_i - \mathbf{U}(1 : i-1, :)\mathbf{c}$;
  $[\rho, p_i] = \max|\mathbf{r}|$;
  $\mathbf{P} \leftarrow [\mathbf{P}, \mathbf{e}_{p_i}]$
end

III. Dynamic Load Model

The dynamic load models in this work are represented by induction motors (IMs) and ZIP loads. The IMs are modeled by 3-rd order differential equations. The state variables are rotor slip $\mathbf{s}$, stator d-axis transient voltage $\mathbf{v'_d}$ and stator q-axis transient voltage $\mathbf{v'_q}$ of all loads. The state space model of all the IMs in a bulk power system can be written as [16],

$$\mathbf{x} = \begin{bmatrix}\mathbf{s} & \mathbf{v'_d} & \mathbf{v'_q}\end{bmatrix}^T \tag{5}$$

$$\mathbf{u} = \mathbf{V_{lbus}} \tag{6}$$

$$\mathbf{A} = \text{diag}(\mathbf{c_l}/\mathbf{2H}, -\omega_s\mathbf{r_r}/\mathbf{X_r}, -\omega_s\mathbf{r_r}/\mathbf{X_r}) \tag{7}$$

$$\mathbf{F}(\mathbf{x}, \mathbf{u}) = \begin{bmatrix}(\mathbf{c_q}(\mathbf{1}-\mathbf{s})^\mathbf{2} - \mathbf{v'_d}\mathbf{I_d} - \mathbf{v'_q}\mathbf{I_q})/\mathbf{2H} \\ -\omega_s\mathbf{r_r}(\mathbf{X_s} - \mathbf{X'_s})\mathbf{I_q}/\mathbf{X_r} + \omega_s\mathbf{s}\mathbf{v'_q} \\ \omega_s\mathbf{r_r}(\mathbf{X_s} - \mathbf{X'_s})\mathbf{I_d}/\mathbf{X_r} + \omega_s\mathbf{s}\mathbf{v'_d}\end{bmatrix} \tag{8}$$

where $\mathbf{H}, \mathbf{X_r}, \mathbf{r_r}, \mathbf{X_s}, \mathbf{X'_s}, \mathbf{c_l}, \mathbf{c_q}, \omega_s$ are the rotor inertia, rotor leakage reactance and resistance, stator synchronous and transient reactances, linear and quadratic load coefficients, synchronous speed, respectively. Note that in (8), $\mathbf{I_d}$ and $\mathbf{I_q}$ are also nonlinear functions of $\mathbf{s}$,

$$\mathbf{I_d} + \mathbf{j}\mathbf{I_q} = \mathbf{V_{lbus}}/(\mathbf{z_{re}} + \mathbf{j}\mathbf{z_{im}}) \tag{9}$$

where,

$$\mathbf{z_{re}} = \mathbf{r_s} + (\mathbf{s}\mathbf{X_r}/\mathbf{r_r})(\mathbf{X_s} - \mathbf{X'_s})/(\mathbf{1} + (\mathbf{s}\mathbf{X_r}/\mathbf{r_r})^\mathbf{2})$$
$$\mathbf{z_{im}} = \mathbf{X'_s} + (\mathbf{X_s} - \mathbf{X'_s})/(\mathbf{1} + (\mathbf{s}\mathbf{X_r}/\mathbf{r_r})^\mathbf{2})$$

The second component in the load model is a ZIP load, which is defined by algebraic equations. This component does not introduce state variables. The constant impedance load is merged into the admittance matrix of the system. The current drawn to the constant current $\mathbf{I_{cc}}$ and constant power loads $\mathbf{I_{cp}}$ are expressed as,

$$\mathbf{I_{cc}} + \mathbf{I_{cp}} = \frac{\mathbf{P_{cc0}} \frac{|\mathbf{V}|}{|\mathbf{V_0}|} - \mathbf{jQ_{cc0}} \frac{|\mathbf{V}|}{|\mathbf{V_0}|} + \mathbf{P_{cp0}} - \mathbf{jQ_{cp0}}}{\mathbf{V}^*} \quad (10)$$

where $\mathbf{V_0}$ is the vector of load voltages at the initialization stage of the simulation; $\mathbf{P_{cc0}}, \mathbf{Q_{cc0}}, \mathbf{P_{cp0}}, \mathbf{Q_{cp0}}$ are the vectors of initial real and active powers of constant current and constant power loads, respectively; $\mathbf{V}$ is the vector of load voltages.

The time evolution of the IM loads' state variables of the IEEE 9-bus system with 3 load buses after a 1-cycle 3-phase fault at bus 1 is shown in Fig. 1. Note that the load state indices have been rearranged to collect the states of the same IM into neighboring states for visualization clarity (i.e. rearrange (5) to $[[s_1, v'_{d1}, v'_{q1}]^T, ..., [s_3, v'_{d3}, v'_{q3}]^T]^T$) The repetitive pattern across different IMs shows that a low-dimensional basis may exist to represent the full dynamics of all IM loads. This observation is verified by the SVD of the state variables. As shown in Fig. 2, the time evolution of the full state space of dynamic loads can be represented by 6 dominant modes with a 10^{-3} truncation threshold.

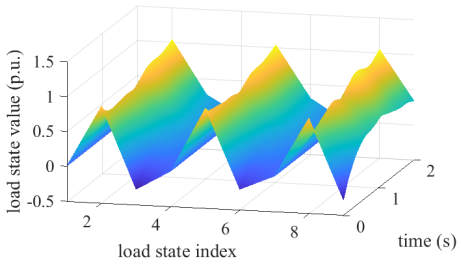

Fig. 1. Manifold of the state variables of IMs defined by $\dot{\mathbf{x}} = \mathbf{A}\mathbf{x} + \mathbf{F}(\mathbf{x}, \mathbf{u})$ at 3 load buses of the IEEE 9-bus system.

However, the SVD of state space only provides a linear approximation of the dynamic loads. To acquire accurate approximation for the nonlinear components, a separate SVD needs to be applied to the nonlinear functions $\mathbf{F}(\mathbf{x}, \mathbf{u})$ of the dynamic load model. The time evolution of the nonlinear functions is shown in Fig. 3. The dominant modes are shown in Fig. 2 alongside those for the state variables. With the same truncation threshold, the nonlinear functions have 7 dominant modes, which suggests that the nonlinear functions have a richer dynamic behavior than the state variables.

After applying Algorithm 1 to the basis acquired from the SVD of the nonlinear functions, the observation points that minimize the projection error of the nonlinear functions onto their basis are selected and highlighted in Fig. 3. It shows that the time evolution of s_1 and s_2 nonlinear functions can be interpolated by the nonlinear function of s_3. Therefore only

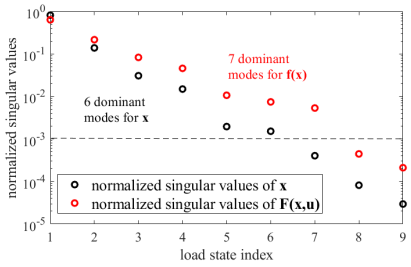

Fig. 2. Normalized singular values of $\mathbf{x}$ and $\mathbf{F}(\mathbf{x}, \mathbf{u})$ for the IMs of the IEEE 9-bus system.

7 out of 9 nonlinear functions need to be evaluated for the ROM.

Another insight provided by the DEIM algorithm is the location of those observation points. For a larger power grid where fine turning all dynamic load models is prohibitively labor-intensive, DEIM observation points can be utilized as suggestions for critical locations for maintaining parameter accuracy. Although for a small system like the IEEE 9-bus system, the observation points cover all three load buses, for a larger system, it is possible to limit the number of observation points to a small number across multiple contingencies. This helps utilities to focus on tuning the critical dynamic load models that contribute the most to accurate ROMs. An example of such benefit is presented in Section V.

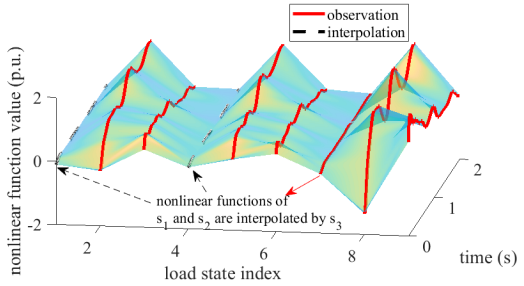

Fig. 3. Apply DEIM to the nonlinear functions $\mathbf{F}(\mathbf{x}, \mathbf{u})$ representing IMs at 3 load buses of the IEEE 9-bus system.

IV. Simulation and System Characteristics

The simulation models for the components other than dynamic load models are 6-th order sub-transient generator models and 1-st order exciter and governor models similar as the ones used in [16]. Their models are kept as full models for all simulations because the subject of model reduction is load model in this work.

Three systems of different scales including the IEEE 9-bus, WECC 179-bus and 2384-bus Polish systems are studied. Their model characteristics are shown in Table I. All the loads in these systems are represented by IM+ZIP.

V. Case Study

A. IEEE 9-bus

As suggested by Fig. 3, there are 7 state variables whose nonlinear functions need to be evaluated for the IEEE 9-bus

TABLE I
SYSTEM CHARACTERISTICS

	9-bus	179-bus	2384-bus
buses	9	179	2384
generator buses	3	29	327
load buses	3	104	1826
branches	6	203	2728
generator states	18	174	981
load states	9	312	5478

system. The simulation result of these state variables using DEIM-POD is compared to the result of using the full model in Fig. 4. It demonstrates a good match for these 7 state variables.

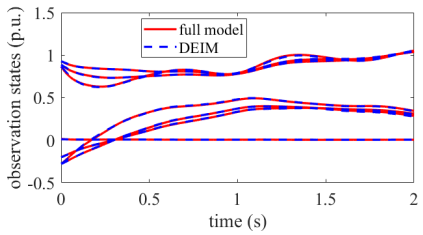

Fig. 4. Observation states comparison of the IEEE 9-bus system's full model and DEIM ROM.

The 2-norm percentage errors of the entire 2-second simulation period for all 9 state variables of the 3 dynamic loads are shown in Fig. 5. It shows that the observation states' errors are minimized as compared to the interpolated states. Note that state 7 (i.e. s_3) has the highest error among all observation states, because it is the last one chosen among all 7 observation states.

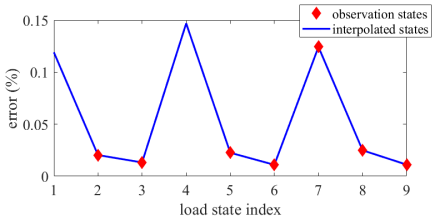

Fig. 5. Normalized error of the IEEE 9-bus system load states simulated using DEIM.

B. WECC 179-bus

The result from WECC 179-bus system demonstrates a significant reduction of nonlinear functions. As shown in Fig. 6, only 7 states' nonlinear functions need to be evaluated to represent the dynamics after a 1-cycle 3-phase fault at bus 1. The 2-norm percentage errors of all 312 load states are shown in Fig. 7.

To show the selected observation points for different contingencies, a total of 179 simulations with 1-cycle 3-phase bus faults applied to each bus in the system are performed. As shown in Fig. 8, only a small number of load buses have states that are frequently selected by DEIM across all

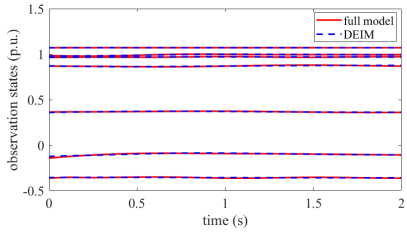

Fig. 6. Observation states comparison of the WECC 179-bus system's full model and DEIM ROM.

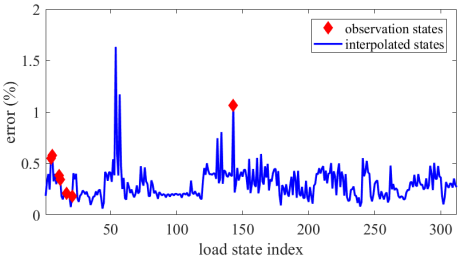

Fig. 7. Normalized error of the WECC 179-bus system load states simulated using DEIM.

contingencies. The load buses that have states selected for at least 40 contingencies are highlighted in Fig. 9. The selected locations provide a comprehensive coverage of the system. It shows that DEIM can indeed be utilized as a means of selecting critical locations for maintaining dynamic load model accuracy.

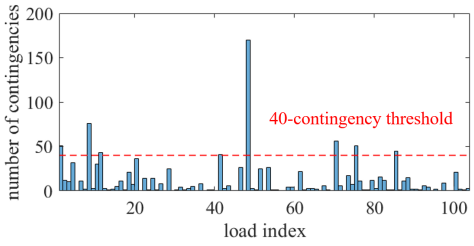

Fig. 8. Number of contingencies for which each load is chosen as observation point in WECC 179-bus system.

C. 2384-bus Polish

For the 2384-bus Polish system, there are 3 selected observation states as shown in Fig. 10 after a 1-cycle 3-phase fault at bus 1. The 2-norm percentage errors of all 5478 load states are shown in Fig. 11 and all of them are maintained under 0.6%.

For 300 1-cycle 3-phase bus faults applied at different locations in the system, the top 3 most frequently selected observation locations are load 45 (300 times), load 247 (30 times) and load 46 (16 times).

D. ROM Characteristics

The ROM characteristics constructed for the dynamics after the 1-cycle 3-phase fault at bus 1 of the 3 studied systems are

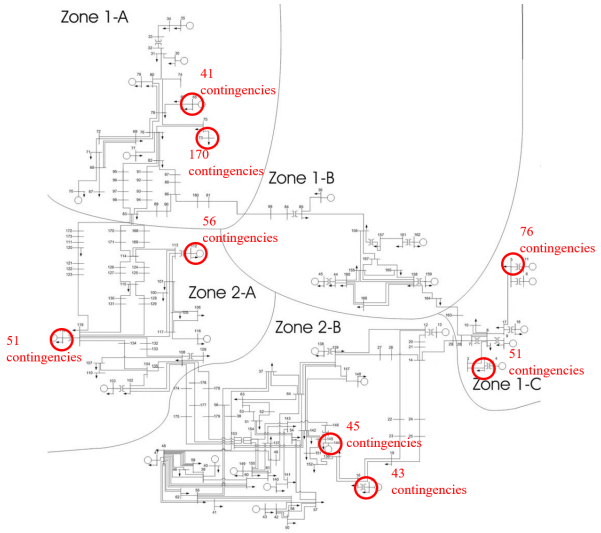

Fig. 9. Locations of load bus most frequently chosen as observation point in WECC 179-bus system.

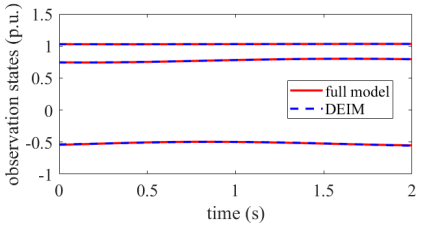

Fig. 10. Observation states comparison of the 2384-bus Polish system's full model and DEIM ROM.

shown in Table II. Although for the IEEE 9-bus system, the number of avoided nonlinear function evaluation is only 2, for the 2384-bus Polish system, the number reaches 5475, which suggests the potential of this approach to large systems.

TABLE II
ROM CHARACTERISTICS OF STUDIED SYSTEMS

	9-bus	179-bus	2384-bus
load state modes	6	3	3
nonlinear function modes	7	7	3
s observation	1	0	0
v'_d observation	3	4	2
v'_q observation	3	3	1
observation load buses	3	5	2
avoided nonlinear evaluations	2	305	5475
nonlinear evaluations without ROM	9	312	5478

VI. CONCLUSION

This work presents a model reduction method for dynamic loads modeled as IM+ZIP. The novelty of this approach is the application of a hyper-reduction method, DEIM, to the nonlinear functions in dynamic load models to sparsely select observation points for evaluation. The observation points can also be utilized to identify critical load locations for maintaining parameter accuracy. This approach limits utilities' effort in maintaining load parameters from the entire system to a small number of locations. In future work, this approach will be extended to construct a library of basis and observation points so that it can be applied to multiple contingencies.

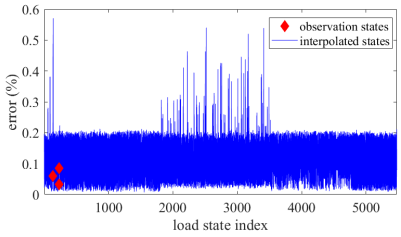

Fig. 11. Normalized error of the 2384-bus Polish system load states simulated using DEIM.

REFERENCES

[1] Z. Ma, Z. Wang, Y. Wang, R. Diao, and D. Shi, "Mathematical representation of wecc composite load model," *Journal of Modern Power Systems and Clean Energy*, vol. 8, no. 5, pp. 1015–1023, 2020.

[2] Y. Zhu and J. V. Milanović, "Automatic identification of power system load models based on field measurements," *IEEE Trans. Power Syst.*, vol. 33, no. 3, pp. 3162–3171, 2018.

[3] A. Arif, Z. Wang, J. Wang, B. Mather, H. Bashualdo, and D. Zhao, "Load modeling—a review," *IEEE Transactions on Smart Grid*, vol. 9, no. 6, pp. 5986–5999, 2018.

[4] J. K. Kim, B. Lee, J. Ma, G. Verbic, S. Nam, and K. Hur, "Understanding and evaluating systemwide impacts of uncertain parameters in the dynamic load model on short-term voltage stability," *IEEE Trans. Power Syst.*, 2020.

[5] J. H. Chow, *Power system coherency and model reduction*. Springer, 2013, vol. 84.

[6] D. Chaniotis and M. A. Pai, "Model reduction in power systems using krylov subspace methods," *IEEE Trans. Power Syst.*, vol. 20, no. 2, pp. 888–894, 2005.

[7] Z. Zhu, G. Geng, and Q. Jiang, "Power system dynamic model reduction based on extended krylov subspace method," *IEEE Trans. Power Syst.*, vol. 31, no. 6, pp. 4483–4494, 2016.

[8] J. Qi, J. Wang, H. Liu, and A. D. Dimitrovski, "Nonlinear model reduction in power systems by balancing of empirical controllability and observability covariances," *IEEE Trans. Power Syst.*, vol. 32, no. 1, pp. 114–126, 2017.

[9] S. Wang, S. Lu, N. Zhou, G. Lin, M. Elizondo, and M. A. Pai, "Dynamic-feature extraction, attribution, and reconstruction (dear) method for power system model reduction," *IEEE Trans. Power Syst.*, vol. 29, no. 5, pp. 2049–2059, 2014.

[10] D. Osipov and K. Sun, "Adaptive nonlinear model reduction for fast power system simulation," *IEEE Trans. Power Syst.*, vol. 33, no. 6, pp. 6746–6754, 2018.

[11] P. Benner, S. Gugercin, and K. Willcox, "A survey of projection-based model reduction methods for parametric dynamical systems," *SIAM review*, vol. 57, no. 4, pp. 483–531, 2015.

[12] S. Chaturantabut and D. C. Sorensen, "Nonlinear model reduction via discrete empirical interpolation," *SIAM J. Sci. Comput.*, vol. 32, no. 5, pp. 2737–2764, 2010.

[13] B. Yildirim, C. Chryssostomidis, and G. Karniadakis, "Efficient sensor placement for ocean measurements using low-dimensional concepts," *Ocean Modelling*, vol. 27, no. 3-4, pp. 160–173, 2009.

[14] M. Barrault, Y. Maday, N. C. Nguyen, and A. T. Patera, "An 'empirical interpolation' method: application to efficient reduced-basis discretization of partial differential equations," *Comptes Rendus Mathematique*, vol. 339, no. 9, pp. 667–672, 2004.

[15] S. L. Brunton and J. N. Kutz, *Data Driven Science & Engineering: Machine Learning, Dynamical Systems, and Control*. Cambridge, England: Cambridge University Press, 2019.

[16] B. Wang, N. Duan, and K. Sun, "A time–power series-based semi-analytical approach for power system simulation," *IEEE Trans. Power Syst.*, vol. 34, no. 2, pp. 841–851, 2019.